View metadata, citation and similar papers at core.ac.uk

brought to you by CORE

provided by Radboud Repository

Radboud Repository

Radboud University Nijmegen

PDF hosted at the Radboud Repository of the Radboud University Nijmegen

The following full text is a preprint version which may differ from the publisher's version.

For additional information about this publication click this link.
http://hdl.handle.net/2066/91864

Please be advised that this information was generated on 2017-12-06 and may be subject to change.

arXiv:1009.2669v2 [cond-mat.mes-hall] 22 Jan 2011

Graphene adhesion on mica: Role of surface morphology

A. N. Rudenko,[1,*] F. J. Keil,[1] M. I. Katsnelson,[2] and A. I. Lichtenstein[3]

[1] *Institute of Chemical Reaction Engineering, Hamburg University of Technology, Eissendorfer Strasse 38, D-21073 Hamburg, Germany*

[2] *Institute for Molecules and Materials, Radboud University Nijmegen, Heijendaalseweg 135, 6525 AJ Nijmegen, The Netherlands*

[3] *Institute of Theoretical Physics, University of Hamburg, Jungiusstrasse 9, D-20355 Hamburg, Germany*

(Dated: January 25, 2011)

We investigate theoretically the adhesion and electronic properties of graphene on a muscovite mica surface using the density functional theory (DFT) with van der Waals (vdW) interactions taken into account (the vdW-DF approach). We found that irregularities in the local structure of cleaved mica surface provide different mechanisms for the mica-graphene binding. By assuming electroneutrality for both surfaces, the binding is mainly of vdW nature, barely exceeding thermal energy per carbon atom at room temperature. In contrast, if potassium atoms are non uniformly distributed on mica, the different regions of the surface give rise to n- or p-type doping of graphene. In turn, an additional interaction arises between the surfaces, significantly increasing the adhesion. For each case the electronic states of graphene remain unaltered by the adhesion. It is expected, however, that the Fermi level of graphene supported on realistic mica could be shifted relative to the Dirac point due to asymmetry in the charge doping. Obtained variations of the distance between graphene and mica for different regions of the surface are found to be consistent with recent atomic force microscopy experiments. A relative flatness of mica and the absence of interlayer covalent bonding in the mica-graphene system make this pair a promising candidate for practical use.

PACS numbers: 73.20.At, 73.22.Pr

I. INTRODUCTION

A monolayer of graphite, commonly known as graphene, is the first truly two-dimensional crystal (one atom thick), which became experimentally available within the last few years.[1,2] Remarkable electronic properties of graphene make this material a promising candidate for a large variety of electronic applications.[3–5]

Usually graphene is deposited on different substrates owing to the peculiarities of preparation techniques.[6,7] The role of substrates and their effect on electronic transport in graphene are actively debated, but are still not clearly understood. Meanwhile, a number of experimental and theoretical studies show that many properties of graphene are strongly dependent on the substrate.[8–10]

Being a two-dimensional crystal, the free standing graphene is not atomically flat but possesses intrinsic corrugations of the structure (ripples), due to thermal bending fluctuations.[11,12] Although scanning tunneling microscopy (STM) and atomic force microscopy (AFM) experiments allow one to reveal corrugations of graphene on insulating surfaces (e.g., SiO_2),[13,14] the existence of intrinsic ripples in substrate-supported graphene is still a subject of discussion. Being supported on a surface, the corrugated graphene structure may simply reflect the conformation between graphene and the underlying substrate. Quite recently it was reported that the intensity of such ripples can be strongly dependent on the substrate on which graphene is deposited.[15] In particular, graphene monolayers display an exceedingly flat structure being placed on a mica surface, which is several times smoother than a SiO_2 surface. This observation means that the ripples, independently on their nature, can be strongly suppressed by interfacial interactions between graphene and an appropriately chosen (flat) substrate. General theoretical models also support this suggestion.[16]

As for the substrate, micas are known to be well suited for fundamental studies as well as for technological purposes owing to their relative atomic smoothness and a large band gap (7.85 eV).[17] These properties make this material a favorable candidate as a substrate for the deposition of graphene in potential graphene-based devices. Although experimental studies propose a strong interfacial binding between graphene and mica resulting from the vdW interaction,[15,18] the nature of such a binding has not been unambiguously established. Details of the binding, such as dependence on the surface morphology, are also unclear.

In this work we examine the adhesion and electronic properties of graphene supported on a muscovite mica surface by means of first-principles methods. By assuming certain atomic disorder of the mica surface we found that binding with graphene can vary significantly from one surface region to another due to the charge-transfer doping of graphene. As a result, graphene might adopt its lattice accordingly, giving rise to a wavy like structure, but such corrugations of the graphene structure turned out to be rather small. An estimation of maximum height variation shows reasonable agreement with topographic data of AFM.[15] We show that the typical electronic structure of graphene remains unperturbed being in contact with the mica surface, which plays an important role in practical applications of graphene. The possible influence of the mica substrate on transport properties of graphene

is also addressed.

The paper is organized as follows. In Secs. II A and II B we briefly describe the computation methods and crystal structures of the investigated systems, respectively. Section III is devoted to the results and their analysis. In Sec. IV we summarize our results.

II. COMPUTATIONAL DETAILS

A. Calculation method

Ground-state energies and electronic density distributions have been calculated using the plane-wave pseudopotential method as implemented in the QUANTUM-ESPRESSO simulation package.[19,20] In order to calculate adsorption energies and properly take into account dispersive interactions, we use the vdW-DF approach proposed by Dion *et al.*[23,24] showing transferability across a broad spectrum of interactions.[25,26] In this method, the exchange-correlation energy functional consists of three parts: (i) the exchange part of the revised Pedrew-Burke-Ernzerhof (revPBE) functional,[27] (ii) the local correlation part of the standard local density approximation (LDA) functional, and (iii) the non local correlation part, incorporating effective many-body density response and allowing treatment of dispersive interactions without any fitting parameters.

In our calculations we employed an energy cutoff of 30 Ry for the plane-wave basis and 300 Ry for the charge density. Self-consistent calculations of the Kohn-Sham equations were carried out imposing the convergence criterion of 10^{-8} Ry. For Brillouin-zone integration, the tetrahedron scheme[21] and ($16 \times 8 \times 1$) Monkhorst-Pack **k**-point mesh[22] were used. A much finer mesh ($48 \times 24 \times 1$) and a Gaussian broadening of 0.02 Ry were used for the density of states (DOS) calculations.

In order to find the ground structural states of the investigated systems we performed a relaxation of the supercell with fixed in-plane lattice parameters. The stop criterion for the relaxation was set to 0.001 Ry/Å, except for the lowermost layer of atoms, whose positions had been fixed. For all the cases under consideration the height of the supercell was chosen to be 50 Å. In order to avoid spurious interaction between images of the supercell in the [001] direction we also used a dipole correction.[28]

B. Surface structures

Graphene has a two-dimensional honeycomb lattice of sp^2-bonded carbon atoms. Although the real structure of graphene is corrugated, the characteristic length of corresponding ripples is around 100 Å,[11,12] which is much larger than the typical length of the supercell used in first-principles calculations. For this reason we do not consider this phenomenon in our work directly.

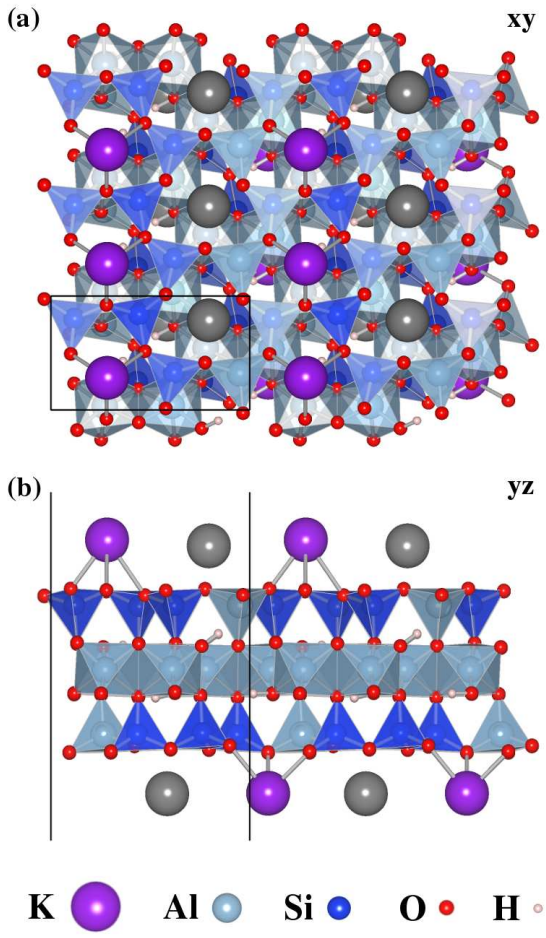

FIG. 1. (Color online) Surface structure of muscovite mica: (a) [001] projection and (b) [100] projection. Depicted structure corresponds to the electroneutral surface with uniform distribution of K^+ ions. Disconnected gray spheres show the positions of extra K^+ ions in the case of an electropositive surface. Black solid lines are the boundaries of the unit cell.

We take into account distortions of carbon lattice caused by non uniformity of the substrate, though these distortions are found to be negligibly small due to the strong sp^2 bonding between carbon atoms and imposed boundary conditions. In general, graphene lattice is not commensurate with the substrate in lateral directions. To overcome this issue we slightly adjust the lateral unit cell parameters of the substrate as described below, bearing in mind that micas have a relative low bulk modulus, i.e., they can be compressed quite easily.[29] We used the lattice constant of graphene equal to $a = 2.459$ Å in accordance with the experimentally obtained value for graphite at low temperatures.[30]

Micas belong to the group of phyllosilicate minerals exhibiting a two-dimensional sheet structure. In this work we examine the surface of muscovite, the most abundant variety of mica. Muscovite is a 2:1 layered dioctahedral aluminosilicate with the formula $KAl_2(Si_3,Al)O_{10}(OH)_2$.[31] Structurally, each irreducible

muscovite layer consists of one layer of octahedrally coordinated Al^{3+} ions, which is sandwiched between two tetrahedral silicate layers with vertices pointing toward the octahedral layer (Fig. 1). Within tetrahedral units aluminum is randomly substituted for silicon with a ratio of 1:3. To compensate the negative charge of adjacent mica layers, potassium counterions are present in 12-fold oxygen coordination.

After the cleavage, half of the potassium ions are assumed to be left to preserve electroneutrality of the surface as a whole. However, the positions of the ions and their distribution over the surface are not well defined from the experimental point of view. Since the interaction between potassium and the surface is of ionic nature, the binding is strong enough to prevent diffusion of potassium ions across the surface at room temperatures. Because lateral diffusion is not possible, a uniform distribution of K^+ cannot be established and, therefore, various regions of the surface could be electrically charged.

Although the ionic surfaces are very reactive and easily adsorb impurities from the environment to neutralize themselves, the existence of uncompensated charges on the mica surface is experimentally verified. Previously, it has been found that the surface potential as well as the surface charge of freshly cleaved mica are sensitively dependent on the environment composition.[32] Moreover, the surface potential of mica cleaved under ultra high vacuum (UHV) conditions is up to two orders of magnitude higher than that for mica cleaved in air.[33] Therefore, we suppose that the strong charging of UHV-cleaved mica is associated with the presence of non uniformly distributed K^+ ions over the mica surface.

To take into account surface-charge effects, we consider the following possibilities for the surface structure: (i) electroneutral structure with uniform distribution of K^+ ions; (ii) electropositive structure with double K^+ coverage; and (iii) electronegative structure in the absence of K^+ ions. We note that for all the cases the whole supercell remains neutral. The change of the surface type is achieved only by varying the concentration of K adatoms and *not* by varying the number of valence electrons in the system.

In the case of the electroneutral substrate, the supercell used in our study consists of a 42-atomic slab of mica and a 16-atomic graphene layer. In order to match graphene and mica supercells, we use a slightly compressed unit cell of mica and employ the following in-plane parameters: $(2 \times 2\sqrt{3})a$, where a is the lattice constant of graphene. This choice corresponds to an ∼6% decrease of the mica experimental lattice constant. The volume of the bulk mica unit cell with given in-plane parameters is about the same as predicted by the LDA.[34] Initial atomic positions for mica were taken from neutron diffraction data,[35] and subsequently relaxed.

It should be noted that there are a number of ways to deposit graphene on the mica surface. In our study we employ the configuration in which lateral coordinates of the topmost potassium atoms on mica are maximally close to that of the center of the carbon hexagon. This choice seems to be reasonable since it corresponds to the most stable configuration of single potassium ions adsorbed on graphene.[36,37]

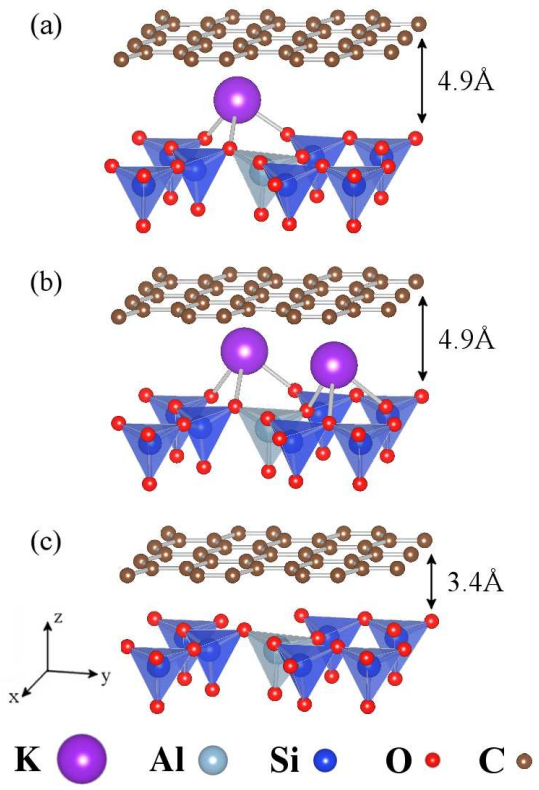

FIG. 2. (Color online) Equilibrium structure of graphene supported on a (a) neutral mica surface, (b) positive mica surface, and (c) negative mica surface. Only the topmost tetrahedral layer of mica is shown.

III. RESULTS AND DISCUSSION

In Fig.2 we show relaxed atomic structures of the mica-graphene interface. One can see that there are no significant changes in the surface structures of mica compared to the bare surfaces (Fig. 1). The only structural parameter affected by the adhesion is the distance between graphene and the topmost oxygen layer of mica. This distance is larger for electroneutral [Fig. 2(a)] and electropositive [Fig. 2(b)] cases due to the presence of K^+ ions on the surface. (Figures 1 and 2 were generated using the VESTA program.[38])

We summarize adhesion energies and equilibrium interlayer distances for graphene adsorbed on mica in Table I. In this table we also show the part of the vdW interaction that contributed to the total energy calculated as a difference between adhesion energies in the presence of the non local correlation functional and without it. As can be seen, the adhesion energies as well as the nature of the interface interaction are strongly dependent on the

TABLE I. Calculated adhesion energies and equilibrium interface distances for graphene supported on a mica surface. Results are given for three different types of mica surfaces as discussed in Sec. II B. Adhesion energies are given in meV per carbon atom. WF and EA correspond to work functions and electron affinities for the bare mica surfaces.

	e^--neutral	e^--positive	e^--negative
E_{adh}, meV/C[a]	-29.3	-75.5	-114.8
vdW part of E_{adh}	92%	69%	53%
d_{eq}, Å[b]	4.9	4.9	3.4
WF, eV	4.15	2.82	9.09
EA, eV	1.25	2.82	9.09

[a] Adhesion energy is calculated in the standard way, i.e. as a difference between the total energies of the mica-graphene system and its isolated components.

[b] Interface distance between graphene and the mica surface implies the difference between averaged z coordinates of carbon atoms in graphene and oxygen atoms in the topmost tetrahedral layer of mica.

surface type. For the electroneutral mica surface the adhesion is caused primarily by the vdW interaction. In this particular case the binding between graphene and the mica surface is quite small in comparison with the interlayer binding in graphite (∼50 meV/C).[39] In the case of both electropositive and electronegative mica surfaces the contributions of the vdW interaction are much smaller than for the neutral surface. Nevertheless, the adhesion energy in these two cases is much stronger than for the neutral case, and exceeds the interlayer binding in graphite. This indicates that there is another mechanism of adhesion besides the vdW interaction.

As has been demonstrated in previous studies, an impurity doping of graphene as well as contact with substrates can lead to an electronic transfer in the system.[36,39–43] Let us consider the possibility of this phenomenon in our case. For two physical systems being in contact the charge transfer occurs if the electronic affinity (EA) of one system is larger than the work function (WF) of the other, if the process is energetically favorable. In Table I we show WFs and EAs for the bare mica surfaces considered, calculated as $(E_{\rm vac} - E_F)$ and $(E_{\rm vac} - E_{\rm cond})$, where $E_{\rm vac}$, E_F, and $E_{\rm cond}$ are the vacuum level of the electrostatic potential, the Fermi energy, and the lowest energy of the conduction band, respectively. Comparing the given values with the graphene WF (which turns out to be equal to EA because of the absence of a band gap) of 4.21 eV, we see that one can expect n-type doping for graphene supported on the electropositive mica surface, p-type doping in the case of the electronegative surface, and also tiny n-type doping in contact with the neutral substrate since the surface WF is almost equal to the graphene EA in this case. Furthermore, one can notice that the larger the difference between the acceptor electron affinity and the donor work function, the larger the obtained adhesion energies. This indicates a significant contribution to the binding between graphene and ionic mica surfaces resulting from the charge transfer.

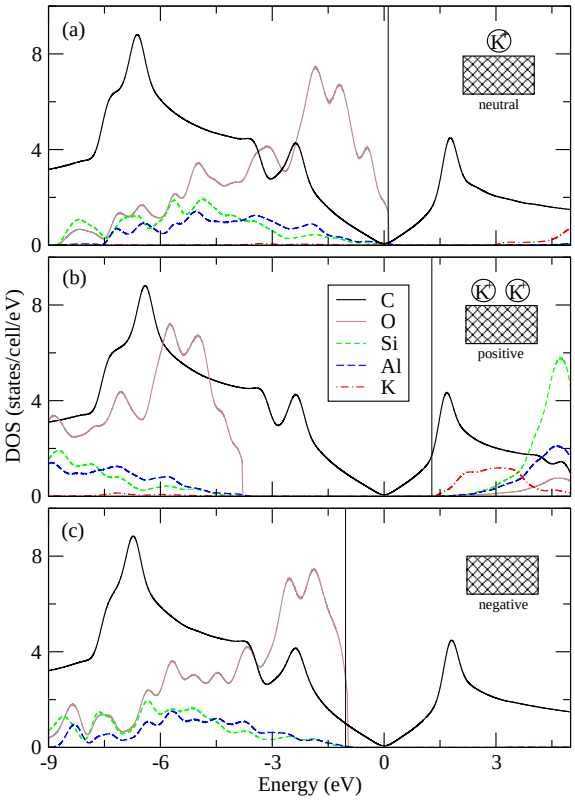

FIG. 3. (Color online) Projected electronic density of states for graphene deposited on the (a) neutral mica surface, (b) positive mica surface, and (c) negative mica surface (see Sec. II B for details). Oxygen DOS is reduced by a factor of 5 for clarity. Zero energy corresponds to the Dirac point of graphene. The vertical line accentuates the Fermi level.

In order to examine electronic transfer and related properties in more detail we analyze the density of electronic states. In Fig. 3 we show the projected DOS on different types of atoms in the supercell for each of the three surfaces with graphene physisorbed: (a) the neutral surface, (b) the surface with one excess electron, and (c) the surface with one excess hole. It is noticeable that for all three cases the typical conical structure of graphene bands in the vicinity of the Fermi level remains unperturbed. This means that in contrast to certain metallic surfaces[42] and adatoms,[36] as well as to some reactive monoatomic adsorbates,[41] the mica surface cannot break the strong sp^2 network of carbon atoms and thereby is not able to form a covalent bonding with graphene. Since the main contribution to the interaction with graphene is defined by the topmost layer of the substrate, the non covalent nature of the mica-graphene binding is consistent with other investigations of graphene interaction with potassium adatoms.[36,37] The fact that the shape of graphene DOS is not altered in contact with the mica surface plays a significant role in terms of the conservation of unique properties of supported graphene. In

this respect the mica surface, having perfect cleavage and atomic smoothness, might be considered as a substrate for potential graphene-based devices.

For the neutral substrate [Fig. 3(a)] the Fermi level lies above the valence band formed by $2p$ electrons of oxygen. In respect to the conical (Dirac) point, the Fermi level is shifted upward by ΔE_F =0.1 eV, which implies only a small electron transfer toward graphene, as expected for inert surfaces. The absence of hybridization and insignificant charge transfer also indicate a vdW nature of relatively weak interaction between graphene and neutral mica surfaces.

For ionic mica surfaces [Figs. 3(a) and 3(b)] there is a distinct shift of the Fermi-level relative to the Dirac point. In the case of positively charged surfaces the electrons are moved toward graphene and the corresponding Fermi-level shift is ΔE_F =1.3 eV. As a result the $4s$ orbital of the topmost potassium layer becomes unoccupied. The opposite situation takes place for the negative surface, where graphene works as a donor causing the Fermi level shift downward by ΔE_F =1.0 eV. Despite the electron transfer from graphene, the oxygen valence band is not completely filled in this case, indicating the presence of unsaturated oxygen electrons in the system. As a rule, the charge transfer leads to ionic interactions between charged constituents of the system. Therefore, besides the vdW interaction one can distinguish two different mechanisms resulting in the binding between graphene and mica, namely, charge transfer and consequent ionic interaction.

Löwdin charge analysis[44] shows the following electron transfers between graphene and mica (in e^-/cell): 0.02, 0.91, and -0.50, respectively, for neutrally, positively, and negatively charged mica surfaces. These values are consistent with previous estimations based on DOS analysis. Non equivalence of the charge transfer for differently charged surfaces allow one to expect an electron-hole asymmetry in graphene supported on realistic mica. Indeed, there is an excess of the electrons transferred from potassium ions toward graphene over the hole transfer from potassium-free regions of mica. On a large scale such asymmetry would produce a shift of the Fermi level toward higher energies relative to the Dirac point. In turn, this may significantly increase the conductivity of mica-supported graphene.

Induced charges in graphene supported on mica might be considered as Coulomb impurities and provide a way for charge-carrier scattering. Recent experiments on potassium-doped graphene demonstrate that carrier mobility is inversely proportional to the concentration of potassium ions on the surface.[45] Moreover, the contribution of potassium ions to the resistivity is maximal for their homogeneous distribution and can be strongly suppressed by clusterization.[46,47] In our case this means that electron mobility should be closely dependent on the particular distribution of potassium ions on mica. However, quantitative analysis of these phenomena requires detailed information about the structure of the mica surface. We leave this question open for further experimental and theoretical studies.

An assumption of a non uniform distribution of potassium atoms on the mica surface provides a mechanism for height variations of graphene supported on mica. As can be seen from Fig. 2 and Table I, the distance from graphene to the topmost tetrahedral layer of mica is larger when potassium atoms are present on the surface. For two limiting cases of high potassium concentration and potassium-free surface the variation of distance is equal to 1.5 Å. As follows from the experimental AFM topographic data,[15] the upper limit of experimentally observed height variations corresponds to our variation of the distance between graphene and the different types of mica surfaces (1.5 Å) with probability around 99%. This correspondence between theoretical results and experimental data allows us to conclude that the irregularity of potassium distribution on the substrate plays a major role in the formation of the graphene corrugations on mica. Intrinsic corrugations of graphene[12] are expected not to exceed height variations caused by these irregularities.

IV. CONCLUSION

We have carried out a first-principles investigation of graphene supported on a muscovite mica surface using the vdW-DF approach. We have shown that an assumption of a non uniform distribution of potassium atoms on the mica substrate may lead to local regions with an uncompensated charge on the surface. In turn, the presence of the surface charges significantly affects the adhesion with graphene. We have found that in the case of the neutral mica surface the interaction with graphene is mainly of a vdW nature, whereas for ionic surfaces there are additional contributions arising from the transfer doping and ionic interaction.

A non uniform distribution of potassium atoms over the surface also provides the main mechanism for variations of graphene height on mica. Our estimations show that the obtained theoretical variations are consistent with recent experimental data.

Finally, it is important that the typical shape of a graphene electronic structure remains unchanged while graphene is deposited on mica. This makes mica a potential candidate for its use as a substrate for graphene-based electronics, in spite of the fact that induced charge impurities may somewhat restrict the unique transport properties of graphene.

V. ACKNOWLEDGMENTS

We would like to thank Tim Wehling for helpful discussions. The authors acknowledge support from the Cluster of Excellence "Nanospintronics" (Hamburg, Germany), from Stichting voor Fundamenteel Onderzoek der

Materie (FOM, the Netherlands) and from the Russian scientific programs No. 02.740.11.0217 and 2.1.1/779.

* rudenko@tu-harburg.de

[1] K. S. Novoselov, A. K. Geim, S. V. Morozov, D. Jiang, Y. Zhang, S. V. Dubonos, I. V. Grigorieva, and A. A. Firsov, Science **306**, 666 (2004).

[2] Andre Geim, APS News **19**(1), 4 (2010).

[3] A. K. Geim and K. S. Novoselov, Nature Mater. **6**, 183 (2007).

[4] A. H. Castro Neto, F. Guinea, N. M. R. Peres, K. S. Novoselov, and A. K. Geim, Rev. Mod. Phys. **81**, 109 (2009).

[5] A. K. Geim, Science **324**, 1530 (2009).

[6] K. S. Novoselov, D. Jiang, F. Schedin, T. J. Booth, V. V. Khotkevich, S. V. Morozov, and A. K. Geim, Proc. Natl. Acad. Sci. U.S.A. **102**, 10451 (2005).

[7] Th. Seyller, A. Bostwick, K. V. Emtsev, K. Horn, L. Ley, J. L. McChesney, T. Ohta, J. D. Riley, E. Rotenberg, and F. Speck, Phys. Stat. Sol. (b) **245**, 1436 (2008).

[8] S. Y. Zhou, G.-H. Gweon, A. V. Fedorov, P. N. First, W. A. de Heer, D.-H. Lee, F. Guinea, A. H. Castro Neto, and A. Lanzara, Nature Mater. **6**, 770 (2007).

[9] T. O. Wehling, A. I. Lichtenstein, and M. I. Katsnelson, Appl. Phys. Lett. **93**, 202110 (2009).

[10] J. Wintterlin and M.-L. Bocquet, Surf. Sci. **603**, 1841 (2009).

[11] J. C. Meyer, A. K. Geim, M. I. Katsnelson, K. S. Novoselov, T. J. Booth, and S. Roth, Nature **446**, 60 (2007).

[12] A. Fasolino, J. H. Los, and M. I. Katsnelson, Nat. Mater. **6**, 858 (2007).

[13] M. Ishigami, J. H. Chen, W. G. Cullen, M. S. Fuhrer, and E. D. Williams, Nano Lett. **7**, 1643 (2007).

[14] V. Geringer, M. Liebmann, T. Echtermeyer, S. Runte, M. Schmidt, R. Rückamp, M. C. Lemme, and M. Morgenstern, Phys. Rev. Lett. **102**, 076102 (2009).

[15] C. H. Lui, L. Liu, K. F. Mak, G. W. Flynn, and T. F. Heinz, Nature **462**, 339 (2009).

[16] T. Li and Z. Zhang, J. Phys. D: Appl. Phys. **43**, 075303 (2010).

[17] A. T. Davidson and A. F. Vickers, J. Phys. C: Solid State Phys. **5**, 879 (1972).

[18] C. Lee, Q. Li, W. Kalb, X.-Z. Liu, H. Berger, R. W. Carpick, and J. Hone, Science **328**, 76 (2010).

[19] P. Giannozzi, S. Baroni, N. Bonini, M. Calandra, R. Car, C. Cavazzoni, D. Ceresoli, G. L. Chiarotti, M. Cococcioni, I. Dabo, A. Dal Corso, S. de Gironcoli, S. Fabris, G. Fratesi, R. Gebauer, U. Gerstmann, C. Gougoussis, A. Kokalj, M. Lazzeri, L. Martin-Samos, N. Marzari, F. Mauri, R. Mazzarello, S. Paolini, A. Pasquarello, L. Paulatto, C. Sbraccia, S. Scandolo, G. Sclauzero, A.P. Seitsonen, A. Smogunov, P. Umari, and R. M. Wentzcovitch, J. Phys.: Condens. Matter, **21**, 395502 (2009).

[20] The pseudopotentials used in this work were taken from QUANTUM-ESPRESSO web page [http://www.quantum-espresso.org].

[21] P. E. Blöchl, O. Jepsen, and O. K. Andersen, Phys. Rev. B. **49**, 16223 (1994).

[22] H. J. Monkhorst and J. D. Pack, Phys. Rev. B. **13**, 5188 (1976).

[23] M. Dion, H. Rydberg, E. Schröder, D. C. Langreth, and B. I. Lundqvist, Phys. Rev. Lett. **92**, 246401 (2004).

[24] T. Thonhauser, V. R. Cooper, S. Li, A. Puzder, P. Hyldgaard, and D. C. Langreth, Phys. Rev. B **76**, 125112 (2007).

[25] D. C. Langreth, B. I. Lundqvist, S. D. Chakarova-Käck, V. R. Cooper, M. Dion, P. Hyldgaard, A. Kelkkannen, J. Kleis, Lingzhu Kong, Shen Li, P. G. Moses, E. Murray, A. Puzder, H. Rydberg, E. Schröder, and T. Thonhauser, J. Phys.: Condens. Matter **21**, 084203 (2009).

[26] C. Ambrosch-Draxl, D. Nabok, P. Puschnig, and C. Meisenbichler, New J. Phys. **11**, 125010 (2009).

[27] Y. Zhang and W. Yang, Phys. Rev. Lett. **80**, 890 (1998).

[28] L. Bengtsson, Phys. Rev. B **59**, 12301 (1999).

[29] J. D. Bass, in *Mineral Physics and Crystallography: A Handbook of Physical Constants*, edited by T. J. Ahrens (American Geophysical Union, Washington, DC, 1995), p.45.

[30] Y. Baskin and L. Meyer, Phys. Rev. **100**, 544 (1955).

[31] M. E. Fleet, *Rock-Forming Minerals. Vol. 3A: Micas*, 2nd ed. (The Geological Society, London, U.K., 2003), p.41.

[32] G. Qi, Y. Yang, H. Yan, L. Guan, Y. Li, X. Qui, and C. Wang, J. Phys. Chem. C **113**, 204 (2009).

[33] F. Ostendorf, C. Schmitz, S. Hirth, A. Kühnle, J. J. Kolodziej, and M. Reichling, Nanotechnology **19**, 305705 (2008).

[34] J. Ortega-Castro, N. Hernández-Haro, V. Timón, C.I. Sainz-Díaz, and A. Hernández-Laguna, American Mineralogist **95**, 249 (2010).

[35] R. Rothbauer, Neues Jahrb. Mineral. Monatsh. **4**, 143 (1971).

[36] K. T. Chan, J. B. Neaton, and M. L. Cohen, Phys. Rev. B **77**, 235430 (2008).

[37] K.-H. Jin, S.-M. Choi, and S. H. Jhi, Phys. Rev. B **82**, 033414 (2010).

[38] K. Momma and F. Izumi, J. Appl. Crystallogr. **41**, 653 (2008).

[39] A. N. Rudenko, F. J. Keil, M. I. Katsnelson, and A. I. Lichtenstein, Phys. Rev. B **82**, 035427 (2010).

[40] J. Dai, J. Yuan, and P. Giannozzi, Appl. Phys. Lett. **95**, 232105 (2009).

[41] T. O. Wehling, M. I. Katsnelson, and A. I. Lichtenstein, Phys. Rev. B **80**, 085428 (2009).

[42] P. A. Khomyakov, G. Giovannetti, P. C. Rusu, G. Brocks, J. van den Brink, and P. J. Kelly, Phys. Rev. B **79**, 195425 (2009).

[43] S. J. Sque, R. Jones, and P. R. Briddon, Phys. Status Solidi A **204**, 3078 (2007).

[44] P. O. Löwdin, J. Chem. Phys. **18**, 365 (1950).

[45] J.-H. Chen, C. Jang, S. Adam, M. S. Fuhrer, E. D. Williams, and M. Ishigami, Nat. Phys. **4**, 377 (2008).

[46] M. I. Katsnelson, F. Guinea, and A. K. Geim, Phys. Rev. B **79**, 195426 (2009)

[47] K. M. McCreary, K. Pi, A. G. Swartz, Wei Han, W. Bao, C. N. Lau, F. Guinea, M. I. Katsnelson, and R. K. Kawakami, Phys. Rev. B **81**, 115453 (2010)